Manuscript …

EPR and CV studies cast further light on the origin of the enhanced hydrogen production through glycerol photoreforming on $CuO:TiO_2$ physical mixtures

Juan Martín-Gómez[1], Jesús Hidalgo-Carrillo[1,*], Vicente Montes[1,2], Rafael C. Estévez-Toledano [1], Juan C. Escamilla[1], Alberto Marinas[1], Francisco J. Urbano[1]

[1]*Departamento de Química Orgánica, Instituto Universitario de Investigación en Química Fina y Nanoquímica (IUNAN), Universidad de Córdoba, Campus de Rabanales, Edificio Marie Curie, E-14071 Córdoba, España*

[2]*Current address: University of Extremadura, Badajoz, Spain, Department of Chemical Engineering and Physical Chemistry, Faculty of Science, University Institute of Water, Climate Change and Sustainability (IACYS)*

*Corresponding author. Tel.: +34 957218623; fax: +34957212066. *E-mail address: jesus.hidalgo@uco.es* (Jesús Hidalgo-Carrillo).

Highlights

- H_2 production via glycerol photoreforming enhanced on $CuO:TiO_2$ physical mixtures
- H_2 production values in the same order as those found for supported noble metals
- EPR studies evidenced the formation of Cu(I) or Cu^0 species on UV irradiation
- CV studies suggested the existence of a CuO to Cu (0) photocatalytic cycle
- Electrons for H_2 generation are first transferred from titania to copper species

Manuscript …

Abstract

Different CuO nanoparticles were synthesized and tested in CuO:TiO_2 physical mixtures for hydrogen production through glycerol photoreforming. CuO alone was inactive whereas its presence in CuO:TiO_2 mixtures significantly improved the photoactivity of TiO_2, with smaller CuO nanoparticles leading to higher hydrogen productions. Results obtained through combination of EPR and CV studies suggested the existence of a Cu(II)-Cu^0 catalytic cycle. Thus, electrons promoted to the conduction band of titania could be used for CuO reduction to Cu which in turn would enable hydrogen production regenerating Cu^{2+} for a new catalytic cycle. All in all, a hydrogen production of 88 $mmol \cdot g^{-1}$ was obtained after 5h on a CuO:TiO_2 (10% w/w) physical mixture which is comparable to that achieved in a previous study under identical reaction conditions on 1.5%Pt/TiO_2.

Keywords: glycerol photoreforming; CuO :TiO_2 physical mixtures; EPR of copper species; CV of copper species.

1. Introduction

The consumption of fossil fuels generates CO_2 along with other pollutants, largely responsible for the greenhouse effect and poor air quality in large cities. Thus, the search for alternative, less pollutant, renewable fuels has become the main goal of researchers on energetic issues. Hydrogen could be part of the solution since its combustion leads to water as the only product [1,2].

Currently, hydrogen is obtained from four main sources: natural gas (48%), oil (30%), coal (18%) and water (4%). The most important hydrogen production methods from water are (photo)electrochemical, photocatalytic, radiolysis, photobiological synthesis, thermolysis and thermochemical processes [3–5]. The photocatalyzed hydrogen production from oxygenated organic compounds (photo-reforming) uses light in the presence of water, at room temperature and anaerobic conditions, to generate gaseous hydrogen and carbon dioxide [6–10]. The fact that the oxygenated organic compounds come from biomass is an advantage over the use of fossil fuels, since the generated CO_2 is what the biomass itself consumed during its growth. Moreover, the process contributes to the reduction of gas emissions such as CO, NOx, SOx, non-methane hydrocarbons, and particulates [11].

Glycerol is considered a suitable feedstock for photoreforming since it is obtained as a by-product during biodiesel production through transesterification reactions [12,13]. According to the literature on glycerol photoreforming on metal/TiO_2 solids [14,15], while cathodic half reaction implies the reduction of protons to molecular hydrogen, anodic half-reactions proceed through three different parallel reaction pathways involving initial oxidation of primary or secondary carbons (forming glyceraldehyde or dihydroxyacetone, respectively) or oxidative C-C scission (forming glycolaldehyde and formaldehyde), the latter being predominant. As the reaction proceeds, different carboxylic acids are formed in the aqueous phase as reaction intermediates (e.g. formic, glycolic and acetic acid) which are responsible for the progressive drop in pH.

Since Fujishima and Honda [16] reported the electrochemical photolysis of water at a TiO_2 electrode, the most used semiconductor for these type of reactions has been titanium dioxide due to its availability, chemical stability, price and endurance to photo-corrosion, one drawback being the rapid recombination of the electron-hole pairs [17,18]. Moreover, as far as hydrogen generation from the water photo-electrolysis is concerned, TiO_2 presents a very low reaction rate and, therefore, a sacrificial agent should be used in order to increase the amount of hydrogen generated.

One of the strategies to overcome the rapid electron-hole recombination rate in titania is to incorporate noble metals which can act as electron sink, thus resulting in an improvement in the hydrogen production capacity [19–21]. In this sense, our research group [22], using glycerol as a sacrificial agent, reported a hydrogen production rate of 23 $mmol \cdot h^{-1} \cdot g_{cat}^{-1}$ for a 3%Au/TiO_2 catalysts or 15 $mmol \cdot h^{-1} \cdot g_{cat}^{-1}$ for 1.5%Pt/TiO_2 with the same experimental device and reaction conditions used in the present manuscript.

However, the high price of noble metals hinders their practical application and has activated the search for alternative non-noble transition metals. One of the most economical alternatives considered is the incorporation of copper, in the form of CuO or Cu_2O, into classical semiconductors such as TiO_2. In this sense, Yu *et al.* [23] reported a production of 1.8 mmol $H_2 \cdot h^{-1} \cdot g_{cat}^{-1}$ on a 8%CuO/TiO_2 catalyst and Reddy *et al.* [24], using a CuO quantum dots decorated titania nanocomposite, achieved a hydrogen production rate of 21.7 mmol H_2 $h^{-1} \cdot g_{cat}^{-1}$ with glycerol as the sacrificial agent. These results demonstrate that CuO/TiO_2 photocatalysts can produce H_2 at similar levels to those obtained with noble metals supported on TiO_2.

Obtaining photocatalysts based on titania-supported CuO can be carried out through different synthesis processes such as deposition-precipitation, impregnation, photodeposition or sol-gel, among others [22,25]. Nevertheless, these incorporation processes complicate the catalyst synthesis and have a negative economic impact on the generated hydrogen.

Regarding the active species, although copper is normally incorporated to TiO_2 in the form of CuO (or Cu_2O), researchers suggest that during the first stages of the photocatalytic process there is a photo-reduction of the Cu^{+2} species to Cu^{+} or Cu^{0} and that these reduced species are responsible for the improvement of the capacity of hydrogen photo-production of CuO/TiO_2 catalysts [26–30].

Some researchers such as Kum *et al*. [31] proposed the use of CuO and TiO_2 physical mixtures as an alternative to supported CuO photocatalysts, with the main advantage of the simplicity of the preparation of the mixture, its versatility and the low cost of semiconductors used with respect to noble metal-based catalysts. The physical mixtures tested led to a hydrogen production of 8.2 $mmol\ h^{-1} \cdot g_{cat}^{-1}$, quite similar to that reported for titania-supported CuO catalysts.

Recently, Maldonado *et al*. [32] have reported the use of CuO:TiO_2 physical mixtures for the production of hydrogen at a pilot plant scale from different organic compounds acting as sacrificial

electron donors, showing similar hydrogen generation capacity to other more expensive noble metal/TiO_2 photocatalysts such as Au/TiO_2, Pt/(TiO_2-N) or Cu/TiO_2.

All in all, there is currently a large literature on the observed synergistic effect of CuO-TiO_2 mixtures (with copper species either supported or in physical mixtures) in both oxidation and reduction processes. Nevertheless, the reaction mechanism requires further studies. As pointed out by Janczarek *et al* [33], there are discrepancies on the nature of the copper oxidation states responsible for the observed synergistic effect and on whether electrons are transferred from copper species to titania or the other way around. Furthermore, it should be clarified if reaction is fully heterogeneous or homogenous (influence of copper ions in suspension).

In the present piece of research, the capacity of hydrogen generation from glycerol photo-reforming using CuO:TiO_2 physical mixtures is studied. The effect on H_2 production of CuO synthesis temperature, subsequent calcination temperature and CuO content is explored. Finally, the study of the origin of the synergistic effect of the addition of CuO to TiO_2 on the ability to photo-produce hydrogen is also addressed using Z-potential measurements, EPR and CV.

2. Experimental

2.1. Materials

Copper acetate, commercial copper (II) oxide and glycerol were purchased from Sigma-Aldrich Chemical Co. (Madrid, Spain). Glacial acetic acid, sodium hydroxide and Hydrochloric acid were purchased from Applichem Panreac ITW (Madrid, Spain). Titanium dioxide (P 25) was purchased from Evonik Industries AG.

2.2. Synthesis of CuO solids

CuO nanoparticles were synthesized according to the method described by Zhu *et al.* [34]. In brief, 75 mL of 0.02 M copper acetate aqueous solution was mixed with 250 µL glacial acetic acid in a round-bottomed flask furnished with a reflux condenser. The solution was heated to 70, 90 and 100 ºC under vigorous stirring. When temperature reached the desired value, 0.2 g of solid NaOH were added at once, giving an intense black precipitate. The temperature and stirring was kept for 30 min. Under these basic conditions, metastable $Cu(OH)_2$ is transformed to CuO [31].

After being cooled to room temperature, the precipitate was centrifuged, washed once with distilled water, then three times with absolute ethanol and finally dried in air at 110 ºC.

The solids thus obtained were calcined at a rate of 1 ºC·min^{-1} from 50ºC to the selected temperature (250, 450 or 650ºC), the final temperature being kept for 4 hours. The final catalyst was named as:

CuO_Synthesis temperature_ Calcination temperature

For comparative purposes, a commercial CuO solid (labelled as CuO_Com) was also used in the present paper.

2.3. Characterization of CuO nanoparticles

The samples were subjected to thermogravimetric and differential thermal analysis (TG-DTA) on a Setaram SetSys 12 instrument. An amount of 40 mg of sample was placed in an alumina crucible and heated at temperatures from 30 to 900°C at a rate of 10°C·min^{-1} under a stream of synthetic air at 40 mL·min^{-1} to measure weight loss.

The specific surface area and pore volume of the samples were determined by nitrogen adsorption-desorption on a Quantachrome Instruments system (Autosorb-iQ-2-MP/XR Quantachrome, USA) at -196ºC. The solids were outgassed at 120ºC before the analysis. The surface area of the materials was determined by the BET method and the pore size distribution by the DJH method with the corrected form of the Kelvin equation.

To study the particle size distribution of samples, Transmission electron microscopy (TEM) images were taken using a JEOL JEM 1400 microscope available at the Central Service for Research Support (SCAI) of the University or Córdoba, and the particle size distribution was determined using ImageJ® software considering at least 250 particles.

Crystal phase identification was done by XRD analysis using a Bruker D8 Discover with a monochromatic source CuKα1 at λ = 1.54 Å radiation over an angular range of 31-42º at a scan speed of 0.18º 2Θ·min^{-1}. Particle size was estimated by using Scherrer equation:

$$L = \frac{0.89 \cdot \lambda}{\beta \cdot \cos\Theta} \quad (1)$$

where, L, is the mean size of crystallite; λ, is the X-ray wavelength; β, corresponds to the full width at half maximum (FWHM) of the diffraction peak; and θ, is the Bragg angle [36].

Band-gap values were determined by diffuse reflectance UV–vis spectroscopy using a Cary 1E (Varian) instrument and polytetraethylene (density = 1 g·cm^{-3} and thickness = 6 mm) as the refence

material. The plot of the modified Kubelka–Munk function $[F(R)\cdot E]^{1/2}$ or $[F(R)\cdot E]^{2}$ for TiO_2 and CuO, respectively, versus the energy of the absorbed light E was used to obtain the value of band gap as described in the literature [37,38].

Surface charge of materials was determined by Z-potential measurement on a Zetasizer Nano ZSP coupled to an MPT-2 autotitrator using NaOH and HCl to modify the pH.

Electron Paramagnetic Resonance (EPR) measurements were performed on a Bruker EMX-Micro X-band spectrometer operating at a frequency of 9.75 GHz. Field frequency modulation, modulation amplitude, and microwave power were set to 100 kHz, 4 G and 0.6 mW, respectively. EPR spectra were recorded at room temperature in a 3 mm inner diameter quartz tube.

Cyclic voltammetry (CV) analyses were performed with an Autolab (Ecochemie model Pgstat 30) instrument attached to a PC with proper software (GPES) for the total control of the experiments and data acquisition. The electrochemical cell used in CV measurements consisted of a conventional three-electrode system, the working electrode of glassy carbon, the counter electrode of platinum and the reference electrode of Ag/AgCl. The CV experiment was conducted in a potential range from 0.6 to -0.6 V at a rate of 0.2 V s^{-1}.

Temperature-programmed reduction (TPR) analyses were performed on a Micromeritics AutoChem II chemisorption analyser. 40 mg of catalysts were placed in the sample holder and submitted to an initial oxidation step (synthetic air flow 20mL·min^{-1} at 150ºC during 30min). Then, the gas flow was changed to Ar and the temperature dropped to 50ºC. Finally, the sample was reduced in a 20 mL·min^{-1} H_2/Ar (5:95) flow. Temperature was ramped between 0 and 600° C at 10°C·min^{-1}. The final temperature was kept for 20 min.

2.4. Photocatalytic experiments

The photocatalytic hydrogen generation experiments were performed in a Pyrex cylindrical doubled-walled immersion well reactor (23 cm long × 5 cm internal diameter, with a total volume of 190 mL) equipped with a gas circulation system (Ar, 5 mL·min^{-1}), and a medium pressure 125 W-Hg lamp (Photochemical Reactors Ltd), used as excitation source, with an incident light intensity of ca. $1.2\cdot10^{-5}$ Einstein·s^{-1}. Reaction temperature was kept at 10ºC during the experiment by circulating thermostated water. In a typical experiment, 65 mg of photo-catalyst (or CuO:TiO_2 physical mixture) were added to 65 mL of a 10% (v/v) glycerol in water solution and the system

was flowed with 5 mL·min^{-1} Ar for 60 min in order to stablish an inert environment, the Ar flow being maintained throughout the experiment. The reaction started when the lamp was switched on, the generated hydrogen being analyzed online by GC-TCD (Agilent Technologies7890 chromatograph using a Supelco Carboxen^{TM} 1010 PLOT fused silica capillary column 30 m long, 0.32 mm ID). Experiments were carried out with pure CuO or TiO_2 solids as well as with CuO:TiO_2 physical mixtures (1:99, 5:95 and 10:90 w/w). The solids were simply weighted together and added to the reaction medium without any prior gentle mixing in a mortar.

For reutilization studies on CuO:TiO_2 (10:90 w/w) sample using commercial CuO (CuO_Com), after 5h of UV irradiation, the catalyst was filtered under vacuum, washed with water and dried in an oven at 110°C overnight. The reactions were repeated several times to have enough sample for both reutilization and TPR studies.

3. Results and discussion

3.1. Synthesis and characterization of CuO nanoparticles

The synthesis of CuO nanoparticles was carried out based on the method described by Zhu *et al*. [34] which allows to obtain CuO NPs of controlled size in a simple and quick way. The original method involves the addition of solid NaOH to a water solution of copper acetate at 100°C to form a precipitate which once filtered, washed and dried at 110 °C, consists of CuO nanoparticles. In the present work, the effect of the NaOH addition temperature (70, 90 or 100ºC) on the size of the obtained CuO nanoparticles was studied. Each solid was synthesized in duplicate, to determine the reproducibility of the method. Table 1 shows the main data associated to the synthesis and characterization of CuO nanoparticles. The yield of the synthesized CuO nanoparticles, increases with the NaOH addition temperature, from 52% for synthesis carried out at 70°C to a maximum yield of 87.5% for the synthesis performed at 100°C.

Table 1. Some of the main features concerning characterization of the CuO solids used in the present study. Yield of the synthetic procedure, weight loss of dried uncalcined CuO solids, surface area, particle and crystalllite sizes (mean diameter) and isoelectric point of calcined CuO NPs.

Catalyst	Yield (%)	S_{BET} (m^2/g)	Particle size (nm)	Crystallite size(nm)	TGA* Weight lost (%)	Isoelectric point
			TEM	XRD		

CuO_Com	-	11	37	17	0	8.3
CuO_70_250	52.0 ± 2.8	71	10	9	4.4	5.4
CuO_90_250	71.5 ± 2.1	76	8	8	8.8	5.0
CuO_100_250	87.5 ± 3.5	111	7	8	2.6	6.5

*These analyses were performed on dried uncalcined samples.

The thermal stability of the CuO solids dried at 110 °C was analyzed by thermogravimetric analysis, the obtained results being shown in Table 1 and Fig. S1. The range of weight loss is between 2.6 and 8.8% and there is no apparent correlation of these weight losses with the CuO synthesis temperature. Regarding the weight loss profile (Fig. S1), there is a very weak first weight loss between 100 and 200°C, which is associated to the elimination of physisorbed water. A more important weight loss takes place at around 230°C being ascribed to the decomposition of acetate residues remaining in the synthesized solid, as described by Pilloni *et al.* [39]. No significant weight loss is observed in the TGA profiles at temperatures above 250 ºC. Based on these results, the solids were further calcined at 250ºC in order to eliminate the acetate residues which could interfere with the photocatalytic process.

X-ray diffraction (XRD) profiles of the resulting solids are shown in Fig. 1. Diffractograms presented signals at 2θ values of 32.6°, 35.6° and 38.8° corresponding to the (110) (-111) and (111) planes, respectively, of the CuO monoclinic crystalline phase (tenorite), (JCPDS card No. 01-089-2529) [40]. From the Scherrer equation (Equation 1), the CuO crystallite size was obtained (Table 1). Crystallite sizes of CuO_x_250 samples are clearly smaller than that of commercial sample (CuO_Com) (8-9 nm and 17 nm, respectively).

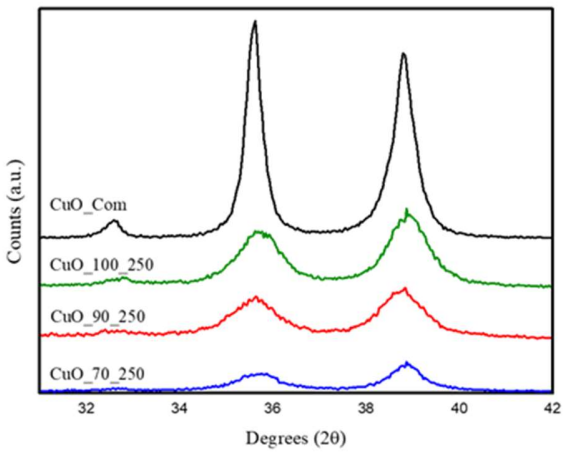

Fig. 1. X-ray diffractograms of commercial and synthesized CuO samples.

TEM results (Fig. 2 and Table 1) suggest that unlike our synthesized CuO NPs whose crystallite (as determined by XRD) and particle (TEM) sizes are quite similar, CuO_Com is constituted by agglomerates of CuO crystallites forming nanoparticles of ca. 37nm. Anyway, in view of the above-presented results, the NaOH addition temperature influences only very slightly the CuO nanoparticle size, with CuO_100_250 (the highest synthesis temperature) leading to the smallest particle size, 7 nm.

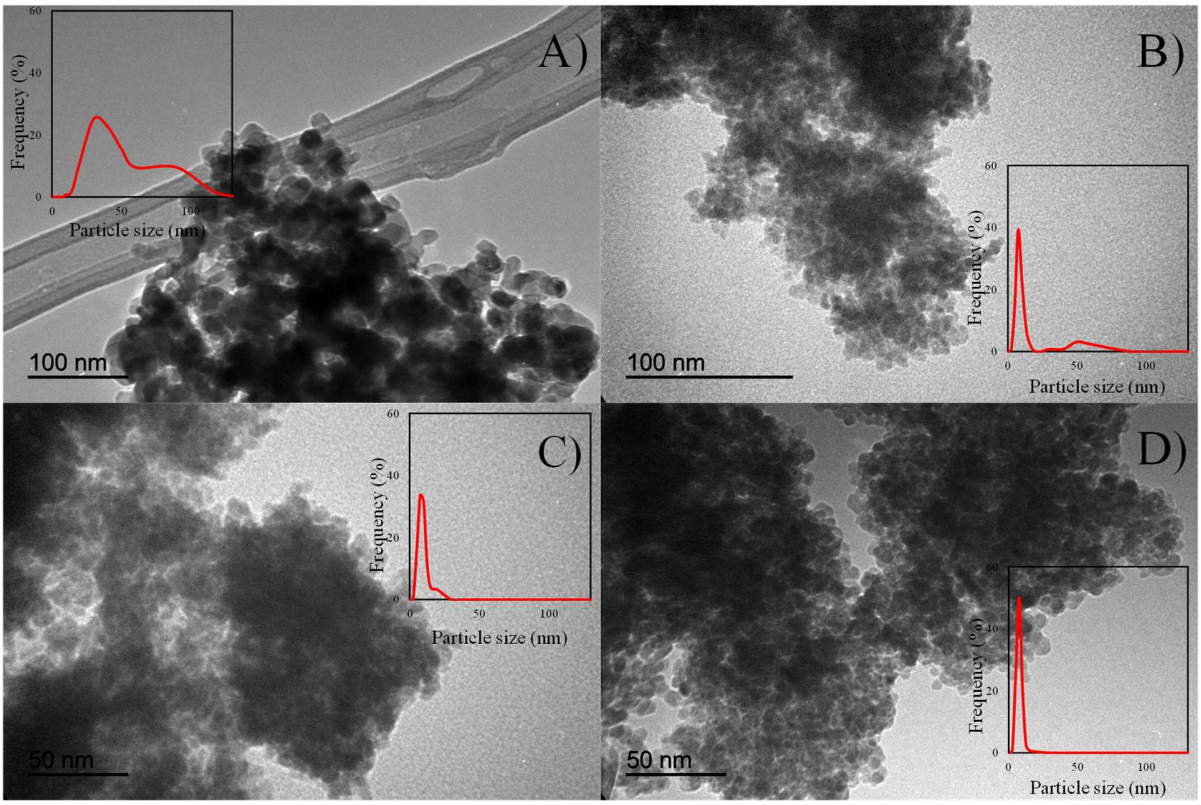

Fig. 2. Transmission electron microscopy (TEM) images of A) CuO_Com, B) CuO_70_250, C) CuO_90_250 and D) CuO_100_250.

242

243 Textural properties of the synthesized CuO nanoparticles were studied by nitrogen adsorption-
244 desorption isotherms. In all cases, type IV isotherms were obtained (Fig. S2). The specific surface
245 area obtained increases with the CuO synthesis temperature from 71 $m^2 \cdot g^{-1}$ for CuO_70_250 to
246 111 $m^2 \cdot g^{-1}$ exhibited by CuO_100_250 (Table 1). The commercial CuO presented quite a low
247 surface area (11 $m^2 \cdot g^{-1}$) in agreement with its larger particle size.

248 Based on the higher yield and surface area obtained for CuO_100_250 solid, the precipitation
249 temperature of 100°C was selected for further studies on the calcination temperature. As discussed
250 from thermogravimetric analyses, a minimum calcination temperature of 250°C is necessary to
251 remove the acetate residues remaining on the uncalcined CuO solid. Taking this temperature as
252 starting point, the CuO_100 material was calcined at 250, 450 and 650°C leading to the
253 CuO_100_250, CuO_100_450 and CuO_100_650 solids.

The solids were studied by means of TEM and XRD to gather additional information on structural properties (Table 2 and Fig. S3). The particle size (mean diameter) of CuO_100_250 nanoparticles, determined by TEM, is only slightly higher than that obtained for the uncalcined CuO_100 (7 and 6 nm, respectively). However, calcination at 450°C and especially at 650°C led to much larger CuO particle sizes, with mean diameters of 36 and 134 nm for CuO_100_450 and CuO100_650 solids, respectively. XRD results confirmed the increase in crystallite size (CuO tenorite) with calcination temperature. Again, higher values are obtained for TEM which as commented previously could be associated to agglomeration of particles.

Table 2. Crystallite and particle size determined by XRD and TEM, respectively, for CuO_100 nanoparticles calcined at different temperatures. TEM images are shown in Fig S3

Catalyst	Particle size (nm)	Crystallite size (nm)
	TEM	XRD
CuO_100	6	6
CuO_100_250	7	8
CuO_100_450	36	20
CuO_100_650	134	36

As for the band gap values of the CuO NPs, they were in the 1.5-1.6 eV range whereas that of TiO_2 Evonik P25 was 3.1 eV. These results are consistent with those reported in the literature [37,41].

3.2. Photocatalytic activity of CuO:TiO_2 physical mixtures in glycerol photo-reforming

The samples were tested for the photocatalytic generation of hydrogen through photoreforming of a 10% in water glycerol solution using UV-light. None of the pure CuO samples (either synthesized or commercial) exhibited any photocatalytic activity under our experimental reaction conditions. As for pure TiO_2 Evonik P25, it showed a small hydrogen generation capacity of 1.9 mmol $H_2 \cdot g^{-1}$ after 5 hours of reaction. CuO:TiO_2 physical mixtures exhibited higher hydrogen productions than TiO_2 Evonik P25. The obtained results are going to be commented now.

3.2.1. Influence of CuO synthesis temperature

An initial screening of the photocatalytic activity obtained on CuO:TiO_2 10:90 w/w physical mixtures was made. Fig. 3 shows the hydrogen generated after 2 and 5 hours of reaction. As can be seen, our synthesized samples exhibited higher hydrogen productions than commercial sample (86-88 mmol·g^{-1} and 52 mmol·g^{-1} after 5h, respectively). Moreover, there is a slight increase in hydrogen production with synthesis temperature (86, 87 and 88 mmol·g^{-1} for CuO_70_250, CuO_90_250 and CuO_100_250, respectively). These small differences are in accordance with those observed in the CuO particle sizes. Thus, the use in the mixtures of CuO_Com NPs with a larger particle diameter (37 nm) led to lower photocatalytic activity while synthesized CuO NPs, with smaller particle diameter (between 7 and 10 nm), showed a greater capacity for hydrogen production. Larger surface area (see Table 1) and higher UV sensitivity of small CuO nanoparticles could account for that.

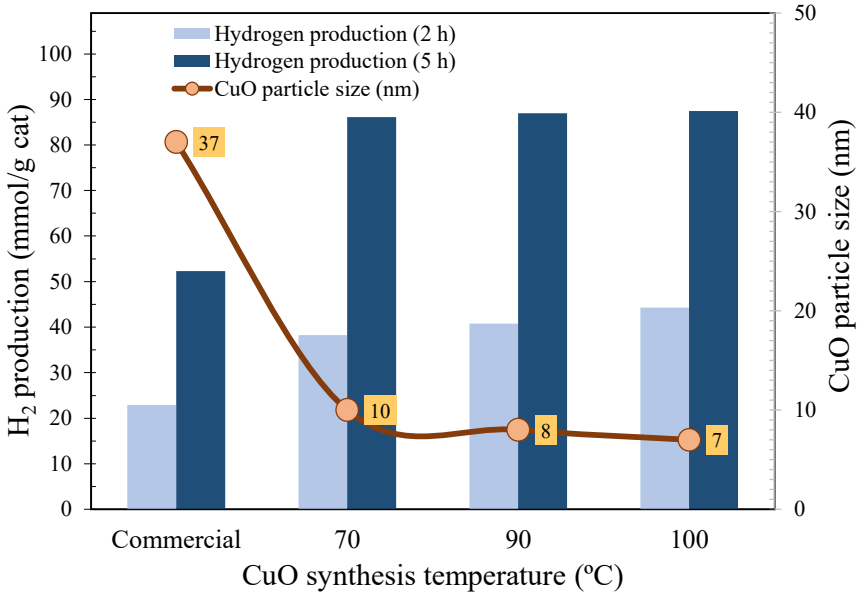

Fig. 3. Influence of the CuO synthesis temperature on the photocatalytic activity of CuO:TiO_2 10/90 w/w physical mixtures. CuO particle size determined by TEM has also been included.

Given that CuO_100_250 was the solid exhibiting the better catalytic results, synthetic temperature of 100ºC was selected for further studies.

3.2.2. Influence of calcination temperature of CuO_100

In order to study the effect of calcination temperature on hydrogen photo-production, CuO_100 sample was calcined at 250, 450 and 650ºC, thus leading to CuO_100_250, CuO_100_450 and CuO_100_650 solids. Fig. 4 shows the hydrogen production data (mmol $H_2 \cdot gcat^{-1}$) after 5 h of reaction using CuO:TiO_2 (1:99 w/w) physical mixtures. As can be seen, uncalcined CuO_100 exhibited the smallest hydrogen production capacity (9 mmol $H_2 \cdot gcat^{-1}$) though higher than that of pure titania (ca. 2 mmol $H_2 \cdot gcat^{-1}$). The low photoactivity of the mixtures containing uncalcined CuO could be due to the presence of residual acetate anion residues. On the other hand, CuO_100_250 led to the greater capacity of hydrogen production in physical mixtures, followed by CuO_100_450 and finally CuO_100_650 which presents an activity level only slightly higher than that of the uncalcined CuO_100. Table 2 and Fig S3 show that the main difference between the mixtures based on CuO_100 calcined at different temperatures is the particle size of the CuO which, as commented above, is directly related to the photo-activity of the tested mixtures. In fact, with the exception of the uncalcined solid, CuO particle size increases with the calcination temperature (up to 134 nm for the CuO_100_650 sample) while the hydrogen production capacity of the solids progressively decreases. Again, a smaller CuO particle size improves the photocatalytic behavior of the tested CuO:TiO_2 physical mixtures.

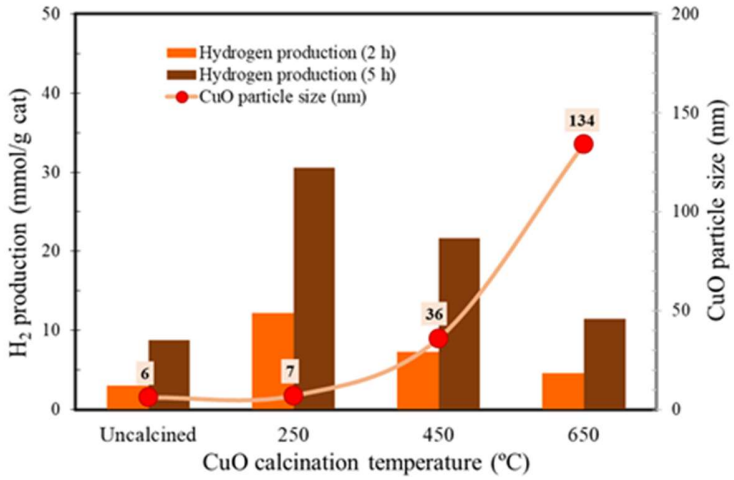

Fig. 4. Influence of CuO_100 calcination temperature on the photocatalytic activity of CuO:TiO_2 physical mixtures (1:99 w/w). CuO particle size determined by TEM.

3.2.3. *Influence of the CuO:TiO_2 ratio in physical mixtures*

Once CuO_100_250 had been found to be the synthetic CuO solid exhibiting the best catalytic performance, its loading in CuO:TiO_2 physical mixtures was optimized. Thus, CuO:TiO_2 physical mixtures with a CuO content of 1, 5 and 10% were tested, the results being presented in Fig. 5. Higher proportions of CuO were ruled out to avoid problems caused by the opacity of the suspension in relation to radiation transmission [42,43]. For comparative purposes physical mixtures with commercial CuO (CuO_Com) were also tested.

Fig. 5A shows a direct relationship between the CuO percentage in the semiconductor mixture and the photocatalytic activity obtained, expressed as mmol $H_2 \cdot gcat^{-1}$. On the other hand, if the capacity of hydrogen generation is expressed per gram of CuO (Fig. 5B), it is observed that the photocatalytic efficiency decreases with increasing the loading of CuO in the mixture. Clearly, an increase in the CuO loading in the mixture does not lead to a directly proportional increase in the hydrogen produced, probably as a consequence of the shielding that an increase in the CuO particles exerts on the incident radiation. Nevertheless, since CuO:TiO_2 ratio of 10:90 w/w was the one producing more hydrogen, it was selected for further experiments expecting to appreciate more clearly the differences found between the catalysts and the effect of changes in reaction conditions.

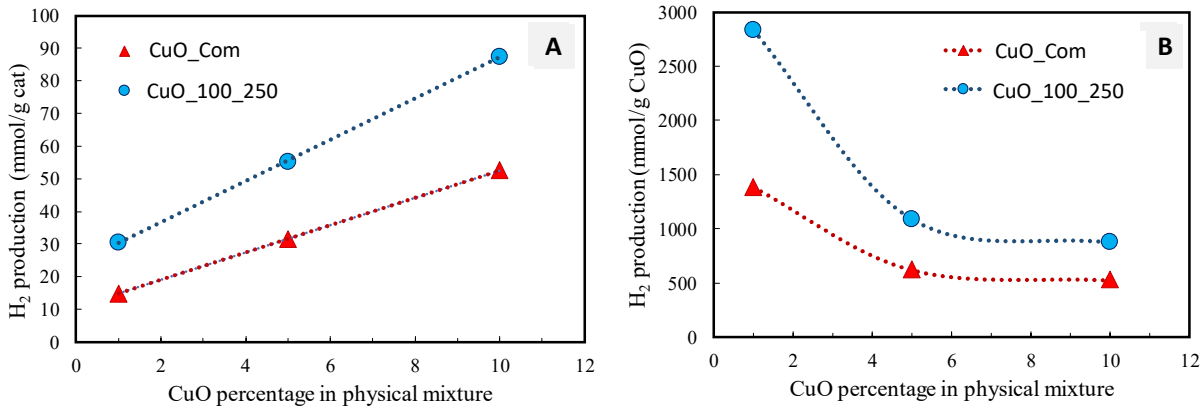

Fig. 5. Influence of the CuO content in CuO:TiO_2 physical mixtures on the hydrogen photogenerated (5h) (A) expressed as hydrogen generated per gram of catalyst; (B) expressed as hydrogen generated per gram of CuO.

3.3. Origin of the enhanced photocatalytic activity of CuO:TiO_2 physical mixtures

As discussed above, CuO samples did not lead to any photocatalytic activity under our experimental activity whereas pure TiO_2 Evonik P25 exhibited a very low activity. In contrast, CuO:TiO_2 physical mixtures presented an enhanced photocatalytic activity. Therefore, the following experiments were designed to cast further light on the reason for that improvement in the photocatalytic production.

Firstly, after 5h of reaction using a CuO_100_250:TiO_2 (10:90 w/w) mixture, the solid was centrifuged and the solution tested for copper and/or titanium leaching by ICP-MS. The results showed that only 3.2% of total Cu had been leached and titanium leaching was negligible. Moreover, the solution was inactive for hydrogen production under our experimental conditions. Therefore, homogeneous catalysis was ruled out.

3.3.1. Zeta potential measurements

Kum *et al.* [31] measured zeta potential of CuO NPs, P25 TiO_2 and other noble metal NPs (Pt, Au, Ag). Only CuO and TiO_2 had opposite charges thus favoring CuO adherence to TiO_2 through electrostatic forces and more uniform attachment to P25. In order to verify if it was the case in our study, both zeta potential (and isoelectric point) of TiO_2 Evonik P25 and synthesized CuO nanoparticles as well as pH evolution during the photocatalytic reaction were measured.

Regarding pH evolution during the reaction, it was monitored over a 5-hour photocatalytic process obtaining the results shown in Fig. 6. In all cases the initial pH of the reaction mixtures consisting of a suspension of CuO:TiO_2 (10:90 w/w) in a 10% aqueous solution of glycerol was between 5.5 and 6.8. Stirring the reaction mixture in the dark for 5h did not produce any variation in the pH value (see dotted blue lines in Fig. 6). However, once the irradiation of the reaction mixture had started, the pH underwent a sharp decrease over the first hour of reaction, reaching pH values between 3.0 and 3.5 and remaining more or less constant for the rest of the process (Fig. 6). The decrease in the pH of the reaction medium under UV irradiation, as commented in the introduction section, is due to the formation of acidic intermediate species such as formic or acetic acids coming from the partial degradation of glycerol [44,45].

Furthermore, the isoelectric point for CuO and TiO_2 was determined separately, from the zeta potential of the solids dispersed in a 10 wt% glycerol aqueous solution, by obtaining the surface charge of the nanoparticles as a function of the pH of the reaction medium. Table 1 shows the isoelectric points obtained for the different CuO NPs, which were between 8.3 for the CuO_Com and 5.0 for the CuO_90_250 solid. Moreover, the isoelectric point obtained for the TiO_2 Evonik P25 was 7.3. The isoelectric points thus obtained are represented in Fig. 6, in green for TiO_2 and in red for CuO, both of them determining the range of pH values for which the CuO and TiO_2 nanoparticles would have opposite electrostatic charges (colored area in Fig. 6). The measurements also showed that absolute value of zeta potentials of NPs throughout the whole pH interval of the experiments was below 30mV for all tested nanoparticles.

Based on the data presented in Fig. 6, the hypothesis of Kum *et al.* [31] on electrostatic attraction between oppositely-charged nanoparticles would be fulfilled only at the very beginning of experiences carried out with Cu_X_250 solids since after ca. 10 minutes, pH dropped at values below the isoelectric points of both CuO and TiO_2 thus being the surface of both solids positively charged. It could be argued that as the reaction proceeds copper oxidation states (as commented below) changes and so the catalyst surface charge. In this sense, strictly speaking, this comment could be only true for t=0 (i.e. the moment when the lamp was switched on and photocatalytic reforming started). Following that reasoning, in the case of experiments with commercial CuO, the surfaces of both CuO_Com and TiO_2 were already positively charged at t=0 and thus not subject to electrostatic attraction phenomena while hydrogen generation occurred. It should be therefore concluded that, at least in that case, the contact between CuO and TiO_2 nanoparticles as was just favored by the fact that the zero potential of NPs is in the -30 to +30 mV range under which circumstances Van der Waals attraction force is larger than electrostatic repulsion [31] .

Once the possibility of the contact between CuO and TiO_2 NPs have been discussed results found for experiments designed to allow us to determine the ultimate origin of the synergistic effect of CuO and TiO_2 physical mixtures on photocatalytic activity are to be commented.

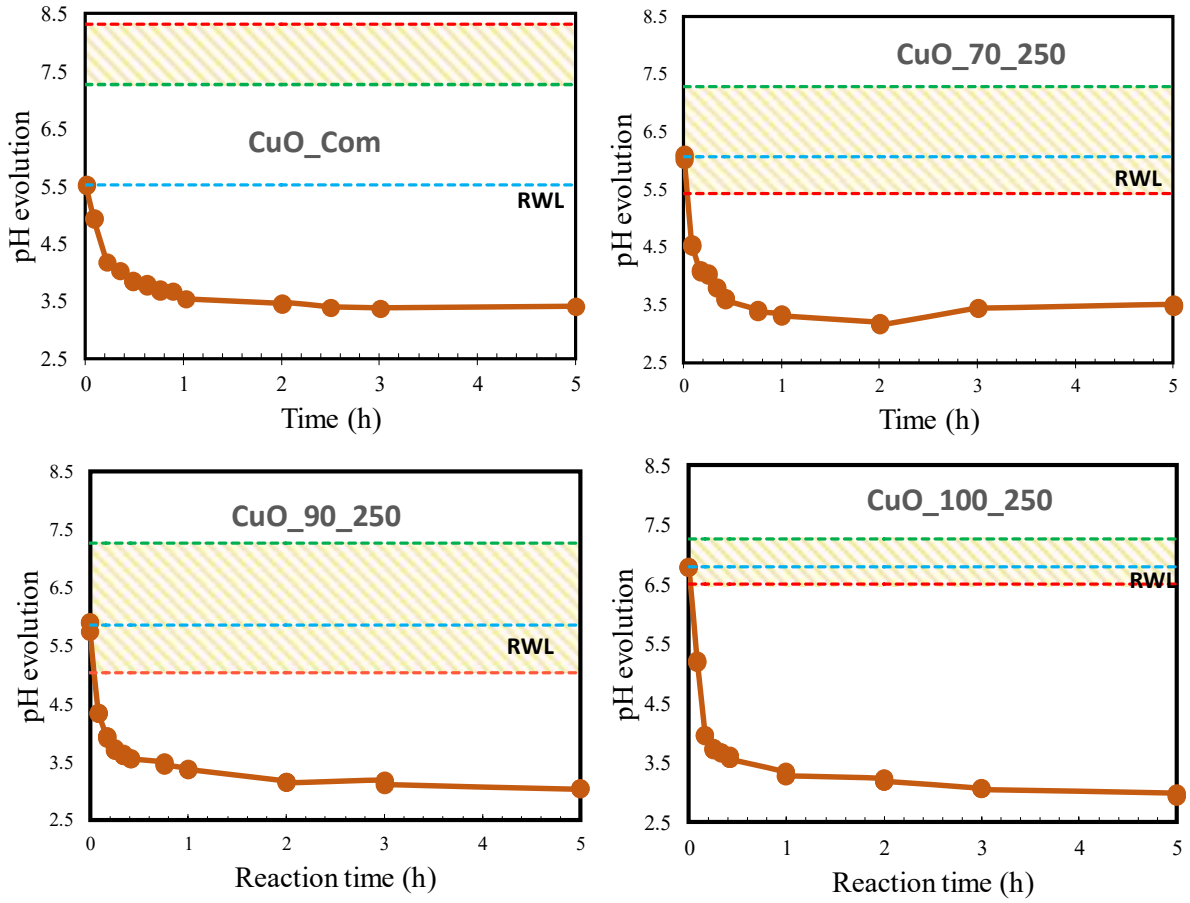

Fig. 6. pH evolution during glycerol photo-reforming (5h) on different CuO:TiO_2 physical mixtures (10:90 w/w). Isoelectric point of pure TiO_2 (green line) and CuO NPs (red line). RWL: pH evolution for the reaction slurry stirred for 5 h in the dark. Shadowed area indicates the zone where CuO and TiO_2 nanoparticles have opposite electrostatic charges.

3.3.2. Active copper species in the photocatalytic reaction

An important fact to understand the synergistic effect of CuO in the physical mixture with TiO_2 is to determine the active copper species that leads to the improvement of the hydrogen generation capacity of TiO_2 in glycerol photoreforming experiments. The CuO synthesis procedure used in this work led, after calcination, to copper in the form of CuO (Cu^{+2}), in its monoclinic tenorite phase, as confirmed by XRD.

Having a look at the literature on hydrogen production through photoreforming on CuO/TiO_2 systems (with copper oxide either supported or just in a physical mixture), it is described that the

irradiation of suspensions of those catalysts results in a pink-purple color [31,46–50]. Nevertheless, there are some discrepancies concerning the origin of the color which is either attributed to trapped electrons in titania [31,48] or to copper nanoparticles [46,47]. Furthermore, there is no general consensus on whether Cu(II) is reduced to Cu(I) [51,52] or Cu^0 [46,47].

In order to cast further light on that, we initially focused our research on determining the oxidation state of the photocatalytically active copper species (Cu^{+2}, Cu^+ or Cu^0) during the reaction, by means of electron paramagnetic resonance (EPR) spectroscopy. EPR is a powerful technique for elucidation of reaction mechanisms in photocatalysis [53,54]. In the case of copper, CuO has paramagnetic properties, showing a wide EPR signal at g= 2.115, while Cu_2O and Cu^0 do not exhibit any EPR signal since they are diamagnetic species [51,52,55].

EPR experiments were carried out by irradiating the analysis probe with UV light, under analogous conditions to those of the photo-catalytic reactions. Initially, the EPR spectrum of the 10% glycerol aqueous solution was recorded, showing a signal at g= 1.93 ascribed to glycerol (Fig. S4). Then, the CuO_Com:TiO_2 physical mixture (10:90, w/w) was added to the 10% aqueous glycerol solution and argon was allowed in to generate inert atmosphere. Under these conditions, the reaction slurry before irradiation was grayish, as shown in Fig. 7A. At the same time, the EPR spectrum of this non-irradiated reaction mixture was recorded, showing, in addition to the above-mentioned signal associated with glycerol, a broad signal at g= 2.19 assigned to CuO nanoparticles (Fig. 7A) [52,55]. Under the same conditions pure TiO_2 did not exhibit such a band (graph not shown).

Once the UV lamp had been switched on and the photocatalytic process started, the slurry progressively turned pink-violet in color (Fig. 7B), in line with the previously commented results described in the literature. Simultaneously, hydrogen generation began as result of glycerol photo-reforming (Fig. 7E). As we mentioned above, the EPR spectrum corresponding to the image in Fig. 7A (gray color) presented signals associated with both glycerol and CuO [56–58] while after 2 hours of reaction (Fig. 7B) the EPR spectrum exclusively showed the signal associated with glycerol, in agreement with the presence of reduced copper species, either Cu_2O or Cu^0 since both are diamagnetic and thus inactive in EPR.

After completing the first 2 hours of reaction, oxygen was allowed into the reaction medium and the UV lamp was turned off, taking the solution a white-grayish color again as a result of the re-

oxidation of the reduced copper species to CuO (Fig. 7C). During this period hydrogen production gradually disappeared (Fig. 7F) and, at the end of the period, the EPR signal associated to CuO [56–58] reappeared, confirming the re-oxidation of copper species (Fig. 7C). At this point, the inert atmosphere was restored by flowing Ar for 30 min and the UV lamp was switched on again, leading to a new change in the color of the slurry to pink-violet (Fig. 7D), the disappearance of the EPR signal associated to the CuO and the recovery of the hydrogen production capacity (Fig. 7G).

These experiments confirm the reversibility of the redox cycle of copper species and the direct relationship of this cycle with the hydrogen production capacity through glycerol photoreforming on CuO:TiO_2 physical mixtures. In any case, it would still be pending to confirm whether the photo-reduction of the CuO leads to Cu^+ (in the form of Cu_2O) or Cu^0.

On the other hand, if the experiment is repeated using pure CuO instead of physical mixture with TiO_2, even in an inert atmosphere and under UV irradiation, the CuO photo-reduction does not take place, and the black color of the initial suspension is maintained, as well as the EPR signal associated to CuO. Moreover, as already commented, under these reaction conditions hydrogen is not generated from glycerol photo-reforming. Thus, these experiments evidence that the presence of TiO_2 in the medium is necessary for the redox cycle of CuO to take place and the generation of hydrogen from photo-reforming process. The photocatalytic activity of CuO:TiO_2 physical mixtures is, therefore, clearly associated with the CuO redox cycle which, in turn, is dependent on CuO-TiO_2 interaction. Under these reaction conditions, for CuO:TiO_2 physical mixtures a synergistic effect is observed that leads to a high hydrogen production capacity, similarly to that reported for metals supported on TiO_2, either based on copper or noble metals. However, the above described experiments do not allow to confirm whether the photo-reduction of the CuO leads to Cu (I) or Cu (0).

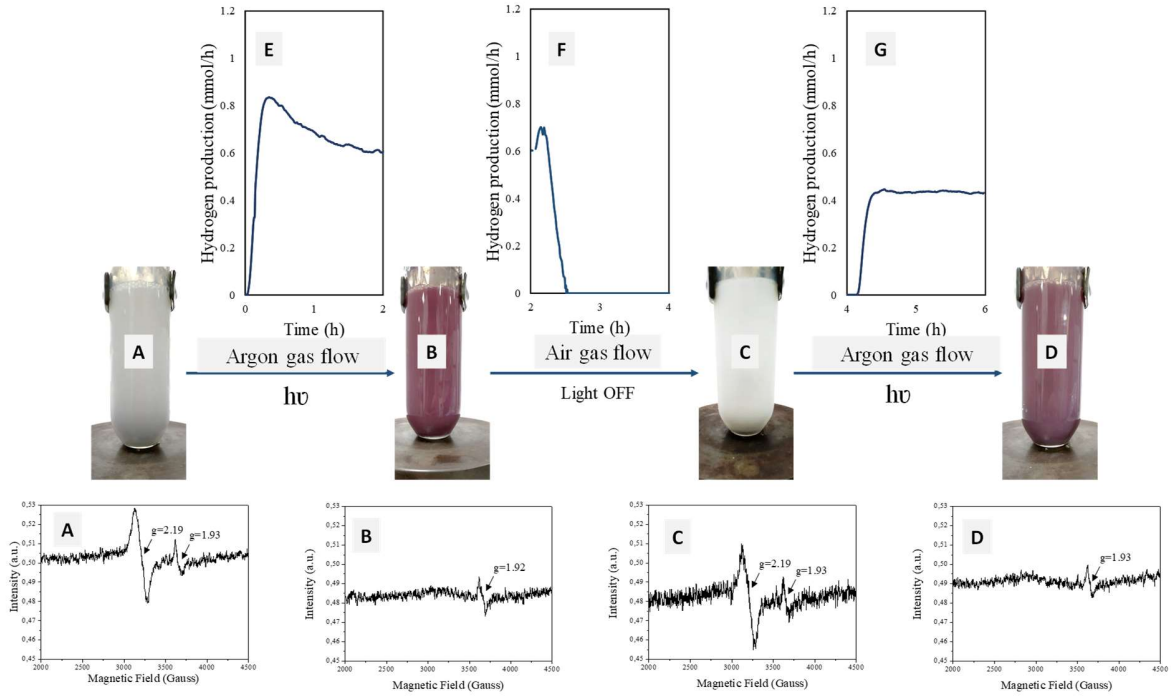

Fig. 7. EPR experiments on a suspension of a CuO_Com:TiO_2 physical mixture (10:90 w/w) in a 10% glycerol in water solution. (A) to (D) Color changes in the slurry and resulting EPR; (E) to (G) Hydrogen production evolution profiles during the experiments.

In order to deepen on the reduction cycle of copper species and, especially, with the aim to determine the oxidation state of Cu active species during UV irradiation (Cu^+ or Cu^0), cyclic voltammetry experiments were carried out. The cyclic voltamperograms (shown in Fig. 8) were recorded applying the potential from cathode to anode (reduction zone), to verify the presence/absence of reduced species. When the potential was applied to the suspension of a CuO_Com:TiO_2 (10:90 w/w) physical mixture (similar conditions to Fig. 7A) from cathode to anode (Fig. 8A, trace 1), a reduction peak appeared at a potential of -0.063 V. Such a peak is ascribed to the reduction from Cu(II) to Cu^0 [59,60]. On the other hand, reversing the process from anode to cathode (oxidation zone, Fig. 8A, trace 2) led to a peak at a potential of 0.025 V which, according to the literature, is due to the Cu(0) to Cu(II) oxidation process [59–61]. Fig. 8B illustrates the same process after irradiation with UV light (similar conditions as Fig. 7B). The absence of peaks in the reduction zone in the first cyclic voltammogram obtained (Fig. 8B trace 1, black line), could confirm the existence of Cu (0) in the irradiated reaction medium.

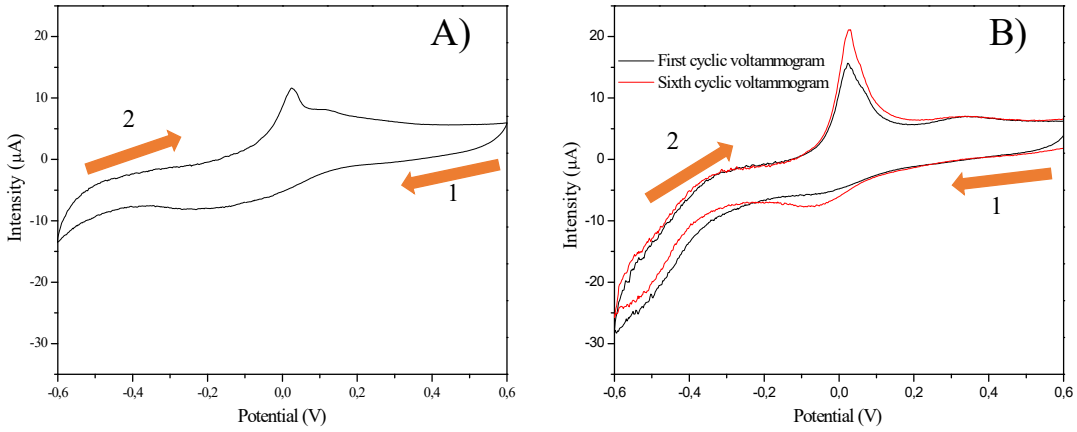

457

458 **Fig.8.** Cyclic voltammograms with at glassy carbon electrode in a 0.1 M KNO_3 solution for (A)
459 CuO_Com:TiO_2 in a glycerol in water solution 10% (v/v) before (A) and after irradiation (B). 1
460 and 2 denote the reduction and oxidation cycle, respectively.

461

462 In contrast, in the reduction zone of the cyclic voltammogram collected after 6 potential cycles
463 (trace 1, red line), in which we start from Cu (II), the Cu (II) to Cu (0) reduction peak appears at a
464 potential of -0.063 V. These direct reduction from Cu(II) to Cu^0 is consistent with that reported in
465 the literature in acidic media [61].

466 The above-described experiments are supportive of the existence of a CuO-Cu-CuO catalytic
467 cycle. However, they do not demonstrate if there is an electron transfer from titania to copper
468 species or the other way around. In order to cast further light on that, a new experiment was carried
469 out, the results being represented in Fig. 9. Therefore, hydrogen evolution during glycerol
470 photoreforming on P25 alone was monitored by MS during 1h. This time was considered long
471 enough as to have reduced states of TiO_2. After that time, the lamp was turned off and 3mL of
472 suspension containing a suspension of CuO-Com in a 10% glycerol in water solution was added.
473 The amount of CuO_Com was calculated as to have a 10:90 w/w TiO_2/CuO mixture in the reaction
474 medium. As can be seen (black trace), the addition of CuO resulted in an increase in hydrogen
475 production which could be indicative of the electron transfer from titania to CuO. Thus CuO would
476 be reduced to Cu which catalyzes the transformation of H^+ into H_2. Obviously, as the lamp was

off, as soon as Cu could not be regenerated through electron transfer from titania conduction band, hydrogen production dropped again. In a blank experiment, once the lamp had been turned off, 3mL of the glycerol solution (without CuO) were added not observing any increase in hydrogen production (see red trace).

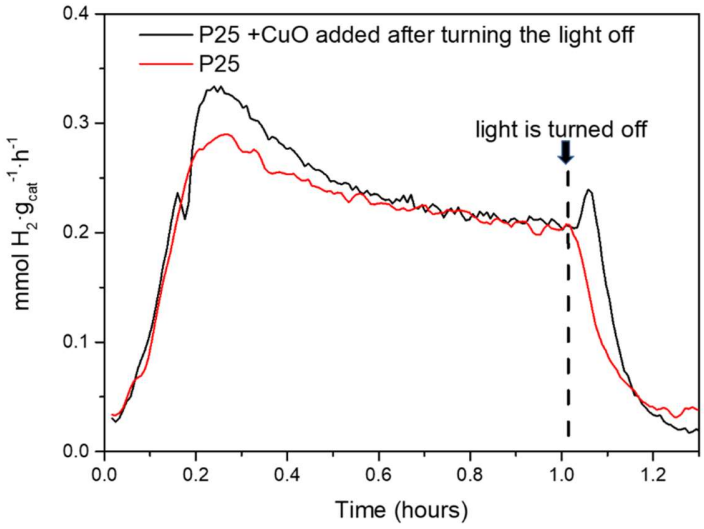

Fig. 9. Experiments designed to evidence the transfer of electrons from titania to CuO during photoreforming of a 10% glycerol in water solution (65mL). Monitoring of hydrogen evolution by MS (m/z=2). Reaction was performed on 58.5mg of TiO_2 P25 for 1h and the lamp was then turned off. Afterwards, 3mL of a 10% glycerol in water solution either alone (red trace) or containing 6.5 mg CuO_com (black trace) was added.

In view of these results, a reaction mechanism is proposed, which is shown in Fig. 10. The incidence of a photon on titania generates the electron-hole pair. Photogenerated electrons are transferred to CuO, which would act as an electron sink, and as a consequence is reduced to Cu(0) thus minimizing the electron-hole recombination. The formed Cu (0) would be responsible for the reduction of protons to H_2 while regenerating the CuO species.

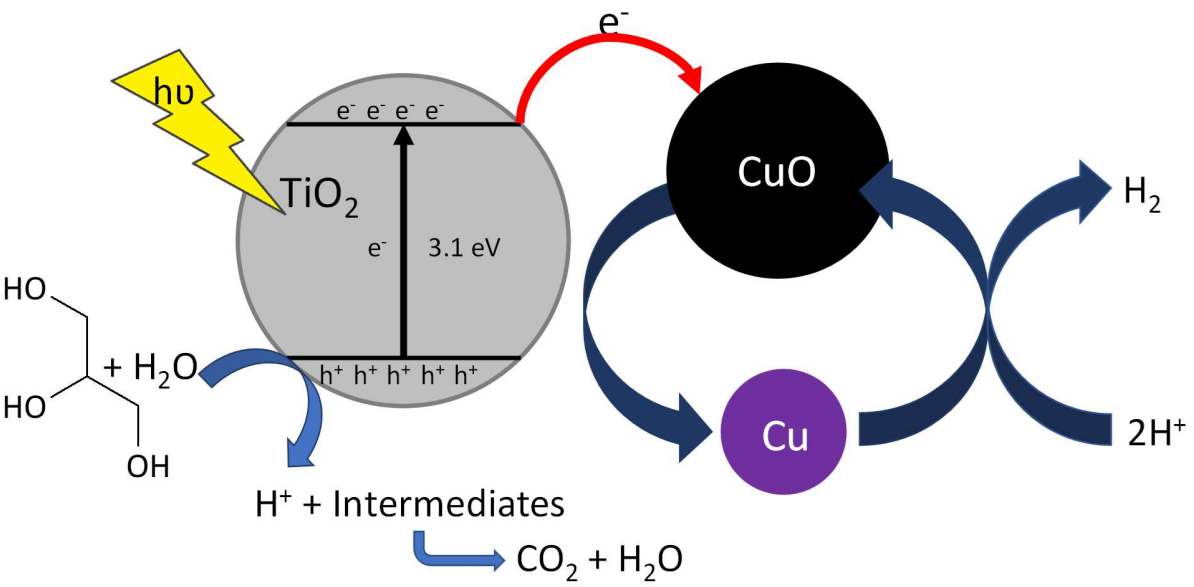

Fig. 10. Proposed reaction scheme for the photo-generation of hydrogen from glycerol reforming over CuO:TiO_2 physical mixtures.

Finally, some reutilization studies were made on CuO_Com:TiO_2 physical mixtures (10:90 w/w), the main results being shown in Fig. 11. Hydrogen production dropped ca. 40% after the first use, whereas it hardly changed in the third consecutive use (Fig. 11A). Complementary studies by TPR evidenced that the copper content felt by 30% (from 10wt% to 6.9wt%) between the first and the second use. As commented above, analysis of the liquid phase by ICP-MS showed that only 3.2% of total Cu had been leached. It is possible that the smallest and more active copper particles were lost during the first filtration. Evolution of TPR profiles (Fig. 11B) evidenced a shift of CuO reduction peak at lower temperatures with the use (from 263ºC for fresh solid to 190-200ºC after uses), which would be supportive of the above-mentioned CuO-TiO_2 interaction during photoreforming.

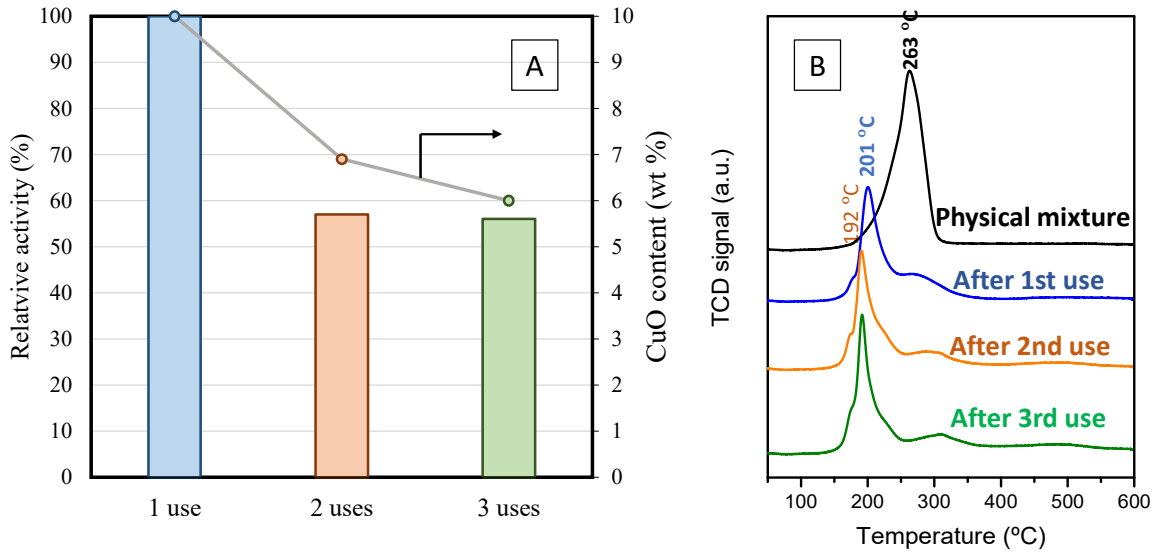

505

506 **Fig. 11**. H_2 photoreforming on CuO_Com:TiO_2 (10:90 w/w) physical mixtures. A) Evolution of relative
507 activity and CuO content (wt %) during reutilization studies, B) TPR of the physical mixture and the catalyst
508 recovered after several uses.

509

510 **4. Conclusions**

511 Different CuO solids were obtained through treatment of copper (II) acetate with NaOH and
512 subsequent calcination. The use of diverse precipitation and calcination temperatures led to CuO
513 solids with different particle sizes. The solids were used in several CuO:TiO_2 physical mixtures
514 and tested for hydrogen photoreforming of glycerol. A synergistic effect of both semiconductors
515 was found with smaller CuO particle sizes leading to higher hydrogen production values.
516 Moreover, experiments on physical mixtures in the 1-10% w/w range showed that even though
517 hydrogen production increases with the CuO content, the highest values expressed per gram of
518 CuO are obtained with the lowest CuO content (1%). EPR experiments evidenced the existence of
519 a catalytic cycle between CuO and either Cu(I) or Cu(0) species. Complementary CV studies
520 suggested that the catalytic cycle is Cu(II)/Cu(0)/Cu(II). Additional experiments evidenced that
521 electrons are transferred from titania to copper species and then to protons for hydrogen gas
522 generation.

523 Synthetic methods for CuO-TiO_2 composites are normally relatively complex, time and energy
524 consuming. In contrast, the use of physical mixtures obviates this step. Therefore, the fact that

525 hydrogen production values are in the same range is particularly interesting. The knowledge of
526 the reaction mechanisms of the physical mixtures CuO and TiO_2 will allow to exploit the potential
527 of the system in the photo-generation of hydrogen.

528 **Acknowledgements**
529 The authors are grateful for the funding received from the Spanish MINECO through the project
530 ENE2016-81013-R (AEI / FEDER, UE) and Spanish MICINN through the project PID2019-
531 104953RB-I00, the Junta de Andalucía and FEDER (P18-RT-4822) and European Social Fund for
532 the Programa Operativo de Empleo Juvenil 2014-2020. Prof. M. Blázquez is also gratefully
533 acknowledged for his help in CV experiments.

534 **Author Contributions.**

535 Funding acquisition, F.J.U. and A.M.; Conceptualization, F.J.U., A.M., V.M. and J.H.-C.;
536 Methodology, A.M., V.M. and J.H.-C.; Investigation, J.H.-C., J.M.-G. Analysis, J.H.-C., J.M.-G.
537 and R.C.E. Writing—Original draft preparation, J.M.-G. and R.C.E.; Writing—Review and
538 editing, A.M., F.J.U., J.H.-C.; Supervision, F.J.U. and A.M. Projects administration, F.J.U. and
539 A.M.

540 **References**

541 [1] J.O.M. Bockris, The origin of ideas on a Hydrogen Economy and its solution to the decay
542 of the environment, Int. J. Hydrogen Energy. 27 (2002) 731–740.
543 https://doi.org/10.1016/S0360-3199(01)00154-9.

544 [2] N. Armaroli, V. Balzani, The hydrogen issue, ChemSusChem. 4 (2011) 21–36.

545 [3] U. Gupta, C.N.R. Rao, Hydrogen generation by water splitting using MoS 2 and other
546 transition metal dichalcogenides, Nano Energy. 41 (2017) 49–65.
547 https://doi.org/10.1016/j.nanoen.2017.08.021.

548 [4] A.A. Basheer, I. Ali, Water photo splitting for green hydrogen energy by green
549 nanoparticles, Int. J. Hydrogen Energy. 44 (2019) 11564–11573.
550 https://doi.org/10.1016/j.ijhydene.2019.03.040.

551 [5] I. Dincer, Green methods for hydrogen production, in: Int. J. Hydrogen Energy, 2012: pp.
552 1954–1971. https://doi.org/10.1016/j.ijhydene.2011.03.173.

[6] H. Bahruji, M. Bowker, P.R. Davies, F. Pedrono, New insights into the mechanism of photocatalytic reforming on Pd/TiO2, Appl. Catal. B Environ. 107 (2011) 205–209.

[7] M. Bowker, Photocatalytic hydrogen production and oxygenate photoreforming, Catal. Letters. 142 (2012) 923–929.

[8] X. Jiang, X. Fu, L. Zhang, S. Meng, S. Chen, Photocatalytic reforming of glycerol for H 2 evolution on Pt/TiO 2: fundamental understanding the effect of co-catalyst Pt and the Pt deposition route, J. Mater. Chem. A. 3 (2015) 2271–2282.

[9] Q. Hao, Y. Song, H. Ji, Z. Mo, X. She, J. Deng, T. Muhmood, X. Wu, S. Yuan, H. Xu, Surface N modified 2D g-C3N4 nanosheets derived from DMF for photocatalytic H2 evolution, Appl. Surf. Sci. 459 (2018) 845–852.

[10] V. Vaiano, M.A. Lara, G. Iervolino, M. Matarangolo, J.A. Navio, M.C. Hidalgo, Photocatalytic H2 production from glycerol aqueous solutions over fluorinated Pt-TiO2 with high {001} facet exposure, J. Photochem. Photobiol. A Chem. 365 (2018) 52–59.

[11] C.C. Elam, C.E.G. Padró, G. Sandrock, A. Luzzi, P. Lindblad, E.F. Hagen, Realizing the hydrogen future: The International Energy Agency's efforts to advance hydrogen energy technologies, Int. J. Hydrogen Energy. 28 (2003) 601–607. https://doi.org/10.1016/S0360-3199(02)00147-7.

[12] K.C. Christoforidis, P. Fornasiero, Photocatalytic Hydrogen Production: A Rift into the Future Energy Supply, ChemCatChem. 9 (2017) 1523–1544. https://doi.org/10.1002/cctc.201601659.

[13] T. Seadira, G. Sadanandam, T.A. Ntho, X. Lu, C.M. Masuku, M. Scurrell, Hydrogen production from glycerol reforming: Conventional and green production, Rev. Chem. Eng. 34 (2018) 695–726. https://doi.org/10.1515/revce-2016-0064.

[14] T. Montini, V. Gombac, L. Sordelli, J.J. Delgado, X. Chen, G. Adami, P. Fornasiero, Nanostructured Cu/TiO 2 photocatalysts for H 2 production from ethanol and glycerol aqueous solutions, ChemCatChem. 3 (2011) 574–577. https://doi.org/10.1002/cctc.201000289.

[15] K.E. Sanwald, T.F. Berto, W. Eisenreich, O.Y. Gutiérrez, J.A. Lercher, Catalytic routes and

581 oxidation mechanisms in photoreforming of polyols, J. Catal. 344 (2016) 806–816.
582 https://doi.org/10.1016/j.jcat.2016.08.009.

583 [16] A. Fujishima, K. Honda, Electrochemical photolysis of water at a semiconductor electrode,
584 Nature. 238 (1972) 37.

585 [17] M. Tahir, N.S. Amin, Indium-doped TiO2 nanoparticles for photocatalytic CO2 reduction
586 with H2O vapors to CH4, Appl. Catal. B Environ. 162 (2015) 98–109.

587 [18] O. Carp, C.L. Huisman, A. Reller, Photoinduced reactivity of titanium dioxide, Prog. Solid
588 State Chem. 32 (2004) 33–177.

589 [19] C.-T. Hsieh, W.-S. Fan, W.-Y. Chen, J.-Y. Lin, Adsorption and visible-light-derived
590 photocatalytic kinetics of organic dye on Co-doped titania nanotubes prepared by
591 hydrothermal synthesis, Sep. Purif. Technol. 67 (2009) 312–318.

592 [20] H. Abdullah, M.M.R. Khan, H.R. Ong, Z. Yaakob, Modified TiO 2 photocatalyst for CO 2
593 photocatalytic reduction: An overview, J. CO2 Util. 22 (2017) 15–32.

594 [21] C.M. Malengreaux, S.L. Pirard, G. Léonard, J.G. Mahy, M. Herlitschke, B. Klobes, R.
595 Hermann, B. Heinrichs, J.R. Bartlett, Study of the photocatalytic activity of Fe 3+, Cr 3+,
596 La 3+ and Eu 3+ single-doped and co-doped TiO 2 catalysts produced by aqueous sol-gel
597 processing, J. Alloys Compd. 691 (2017) 726–738.

598 [22] F.J. López-Tenllado, J. Hidalgo-Carrillo, V. Montes, A. Marinas, F.J. Urbano, J.M.
599 Marinas, L. Ilieva, T. Tabakova, F. Reid, A comparative study of hydrogen photocatalytic
600 production from glycerol and propan-2-ol on M/TiO2 systems (M= Au, Pt, Pd), Catal.
601 Today. 280 (2017) 58–64.

602 [23] J. Yu, Y. Hai, M. Jaroniec, Photocatalytic hydrogen production over CuO-modified titania,
603 J. Colloid Interface Sci. 357 (2011) 223–228. https://doi.org/10.1016/j.jcis.2011.01.101.

604 [24] N.L. Reddy, S. Emin, V.D. Kumari, S. Muthukonda Venkatakrishnan, CuO Quantum Dots
605 Decorated TiO2 Nanocomposite Photocatalyst for Stable Hydrogen Generation, Ind. Eng.
606 Chem. Res. 57 (2018) 568–577. https://doi.org/10.1021/acs.iecr.7b03785.

607 [25] W.-J. Ong, L.-L. Tan, S.-P. Chai, S.-T. Yong, A.R. Mohamed, Highly reactive {001} facets

608 of TiO 2-based composites: synthesis, formation mechanism and characterization,
609 Nanoscale. 6 (2014) 1946–2008.

610 [26] M. Jung, J. Scott, Y.H. Ng, Y. Jiang, R. Amal, CuOx dispersion and reducibility on TiO2
611 and its impact on photocatalytic hydrogen evolution, Int. J. Hydrogen Energy. 39 (2014)
612 12499–12506. https://doi.org/10.1016/j.ijhydene.2014.06.020.

613 [27] M. Jung, J. Scott, Y.H. Ng, Y. Jiang, R. Amal, Impact of Cu oxidation state on
614 photocatalytic H2 production by Cu/TiO2, in: 2014 Int. Conf. Nanosci. Nanotechnol.
615 (ICONN 2014), Institute of Electrical and Electronics Engineers (IEEE), Adelaide
616 (Australia), 2014: pp. 4–6.

617 [28] G.D. Moon, J.B. Joo, I. Lee, Y. Yin, Decoration of size-tunable CuO nanodots on TiO2
618 nanocrystals for noble metal-free photocatalytic H2 production, Nanoscale. 6 (2014)
619 12002–12008. https://doi.org/10.1039/c4nr03521f.

620 [29] L. Sinatra, A.P. Lagrow, W. Peng, A.R. Kirmani, A. Amassian, H. Idriss, O.M. Bakr, A
621 Au/Cu2O-TiO2 system for photo-catalytic hydrogen production. A pn-junction effect or a
622 simple case of in situ reduction?, J. Catal. 322 (2015) 109–117.
623 https://doi.org/10.1016/j.jcat.2014.11.012.

624 [30] Z. Xi, C. Li, L. Zhang, M. Xing, J. Zhang, Synergistic effect of Cu2O/TiO2 heterostructure
625 nanoparticle and its high H2 evolution activity, Int. J. Hydrogen Energy. 39 (2014) 6345–
626 6353. https://doi.org/10.1016/j.ijhydene.2014.01.209.

627 [31] J.M. Kum, S.H. Yoo, G. Ali, S.O. Cho, Photocatalytic hydrogen production over CuO and
628 TiO2 nanoparticles mixture, Int. J. Hydrogen Energy. 38 (2013) 13541–13546.
629 https://doi.org/10.1016/j.ijhydene.2013.08.004.

630 [32] M.I. Maldonado, E. Saggioro, J. Peral, E. Rodríguez-Castellón, J. Jiménez-Jiménez, S.
631 Malato, Hydrogen generation by irradiation of commercial CuO + TiO2 mixtures at solar
632 pilot plant scale and in presence of organic electron donors, Appl. Catal. B Environ. 257
633 (2019) 117890. https://doi.org/10.1016/J.APCATB.2019.117890.

634 [33] M. Janczarek, E. Kowalska, On the Origin of Enhanced Photocatalytic Activity of Copper-
635 Modified Titania in the Oxidative Reaction Systems, Catalysts. 7 (2017) 317.

https://doi.org/10.3390/catal7110317.

[34] J. Zhu, D. Li, H. Chen, X. Yang, L. Lu, X. Wang, Highly dispersed CuO nanoparticles prepared by a novel quick-precipitation method, Mater. Lett. 58 (2004) 3324–3327.

[35] Y. Cudennec, A. Lecerf, The transformation of Cu(OH)2 into CuO, revisited, Solid State Sci. 5 (2003) 1471–1474. https://doi.org/10.1016/j.solidstatesciences.2003.09.009.

[36] M. Sundararajan, P. Sakthivel, A.C. Fernandez, Structural, optical and electrical properties of ZnO-ZnS nanocomposites prepared by simple hydrothermal method, J. Alloys Compd. 768 (2018) 553–562.

[37] J.F. Guayaquil-Sosa, B. Serrano-Rosales, P.J. Valadés-Pelayo, H. de Lasa, Photocatalytic hydrogen production using mesoporous TiO2 doped with Pt, Appl. Catal. B Environ. 211 (2017) 337–348. https://doi.org/10.1016/j.apcatb.2017.04.029.

[38] S. Mavengere, S.C. Jung, J.S. Kim, Visible light photocatalytic activity of NaYF4:(Yb,Er)-CuO/TiO2 composite, Catalysts. 8 (2018) 1–15. https://doi.org/10.3390/catal8110521.

[39] M. Pilloni, V.B. Kumar, G. Ennas, Z. Porat, A. Scano, V. Cabras, A. Gedanken, Formation of metallic silver and copper in non-aqueous media by ultrasonic radiation, Ultrason. Sonochem. 47 (2018) 108–113. https://doi.org/10.1016/j.ultsonch.2018.04.018.

[40] Sathish, S.M. Rafi, H. Shaik, P. Madhavi, Y.R. Kosuri, S.A. Sattar, K.N. Kumar, Critical investigation on Cu-O bonding configuration variation in copper-oxide thin films for low-cost solar cell applications, Mater. Sci. Semicond. Process. 96 (2019) 127–131. https://doi.org/10.1016/j.mssp.2019.02.023.

[41] L. Dörner, C. Cancellieri, B. Rheingans, M. Walter, R. Kägi, P. Schmutz, M. V. Kovalenko, L.P.H. Jeurgens, Cost-effective sol-gel synthesis of porous CuO nanoparticle aggregates with tunable specific surface area, Sci. Rep. 9 (2019) 1–13. https://doi.org/10.1038/s41598-019-48020-8.

[42] I. Tseng, W. Chang, J.C.S. Wu, Photoreduction of CO2 using sol–gel derived titania and titania-supported copper catalysts, Appl. Catal. B Environ. 37 (2002) 37–48. https://doi.org/10.1016/S0926-3373(01)00322-8.

663 [43] P.N. Paulino, V.M.M. Salim, N.S. Resende, Zn-Cu promoted TiO2 photocatalyst for CO2
664 reduction with H2O under UV light, Appl. Catal. B Environ. 185 (2016) 362–370.
665 https://doi.org/10.1016/j.apcatb.2015.12.037.

666 [44] K.E. Sanwald, T.F. Berto, W. Eisenreich, O.Y. Gutiérrez, J.A. Lercher, Catalytic routes and
667 oxidation mechanisms in photoreforming of polyols, J. Catal. 344 (2016) 806–816.
668 https://doi.org/10.1016/j.jcat.2016.08.009.

669 [45] Z. Barbieriková, D. Dvoranová, V. Brezová, Photoinduced transformation of glycerol in
670 titania suspensions. (An EPR spin trapping study of radical intermediates), Catal. Today.
671 313 (2018) 106–113. https://doi.org/10.1016/j.cattod.2017.12.005.

672 [46] M. Imizcoz, A. V. Puga, Optimising hydrogen production: Via solar acetic acid
673 photoreforming on Cu/TiO 2, Catal. Sci. Technol. 9 (2019) 1098–1102.
674 https://doi.org/10.1039/c8cy02349b.

675 [47] H. Tian, X.L. Zhang, J. Scott, C. Ng, R. Amal, TiO2-supported copper nanoparticles
676 prepared via ion exchange for photocatalytic hydrogen production, J. Mater. Chem. A. 2
677 (2014) 6432–6438. https://doi.org/10.1039/c3ta15254e.

678 [48] J. Bandara, C.P.K. Udawatta, C.S.K. Rajapakse, Highly stable CuO incorporated TiO2
679 catalyst for photocatalytic hydrogen production from H2O, Photochem. Photobiol. Sci. 4
680 (2005) 857–861. https://doi.org/10.1039/b507816d.

681 [49] Q. Hu, J. Huang, G. Li, J. Chen, Z. Zhang, Z. Deng, Y. Jiang, W. Guo, Y. Cao, Effective
682 water splitting using CuO x /TiO 2 composite films: Role of Cu species and content in
683 hydrogen generation, Appl. Surf. Sci. 369 (2016) 201–206.
684 https://doi.org/10.1016/j.apsusc.2016.01.281.

685 [50] D. Praveen Kumar, M. V. Shankar, M. Mamatha Kumari, G. Sadanandam, B. Srinivas, V.
686 Durgakumari, Nano-size effects on CuO/TiO2 catalysts for highly efficient H2 production
687 under solar light irradiation, Chem. Commun. 49 (2013) 9443–9445.
688 https://doi.org/10.1039/c3cc44742a.

689 [51] A.A. Samokhvalov, T.I. Arbusova, N.A. Viglin, S. V. Naumov, V.R. Galakhov, D.A.
690 Zatsepin, Y.A. Kotov, O.M. Samatov, D.G. Kleshchev, Paramagnetism in copper monoxide

systems, Phys. Solid State. 40 (1998) 268–271. https://doi.org/10.1134/1.1130290.

[52] A. Viano, S.R. Mishra, R. Lloyd, J. Losby, T. Gheyi, Thermal effects on ESR signal evolution in nano and bulk CuO powder, J. Non. Cryst. Solids. 325 (2003) 16–21. https://doi.org/10.1016/S0022-3093(03)00317-X.

[53] Y. Yan, W. Shi, W. Peng, Y. Lin, C. Zhang, L. Li, Y. Sun, H. Ju, J. Zhu, W. Ma, J. Zhao, Proton-free electron-trapping feature of titanium dioxide nanoparticles without the characteristic blue color, Commun. Chem. 2 (2019) 1–7. https://doi.org/10.1038/s42004-019-0191-7.

[54] Y. Yan, W. Shi, Z. Yuan, S. He, D. Li, Q. Meng, H. Ji, C. Chen, W. Ma, J. Zhao, The formation of Ti-H species at interface is lethal to the efficiency of TiO2-based dye-sensitized devices, J. Am. Chem. Soc. 139 (2017) 2083–2089. https://doi.org/10.1021/jacs.6b12324.

[55] Y. Liu, Z. Ye, D. Li, M. Wang, Y. Zhang, W. Huang, Tuning CuO x -TiO 2 interaction and photocatalytic hydrogen production of CuO x /TiO 2 photocatalysts via TiO 2 morphology engineering, Appl. Surf. Sci. 473 (2019) 500–510. https://doi.org/10.1016/j.apsusc.2018.12.177.

[56] G.F. Lenz, R.A. Bini, T.P. Bueno, R.J. de Oliveira, J.F. Felix, R. Schneider, Self-supported copper (Cu) and Cu-based nanoparticle growth by bottom-up process onto borophosphate glasses, J. Mater. Sci. 52 (2017) 6635–6646. https://doi.org/10.1007/s10853-017-0899-7.

[57] M. Fang, R. Zheng, Y. Wu, D. Yue, X. Qian, Y. Zhao, Z. Bian, CuO nanosheet as a recyclable Fenton-like catalyst prepared from simulated Cu(ii) waste effluents by alkaline H 2 O 2 reaction, Environ. Sci. Nano. 6 (2019) 105–114. https://doi.org/10.1039/c8en00930a.

[58] K. Kappis, C. Papadopoulos, J. Papavasiliou, J. Vakros, Y. Georgiou, Y. Deligiannakis, G. Avgouropoulos, Tuning the catalytic properties of copper-promoted nanoceria via a hydrothermal method, Catalysts. 9 (2019). https://doi.org/10.3390/catal9020138.

[59] S.D. Giri, A. Sarkar, Electrochemical study of bulk and monolayer copper in alkaline solution, J. Electrochem. Soc. 163 (2016) H252–H259.

719 https://doi.org/10.1149/2.0071605jes.

720 [60] A.A. Shaikh, M. Badrunnessa, J. Firdaws, M.S. Rahman, N.A. Pasha, P.K. Bakshi, A cyclic
721 voltammetric study of the influence of supporting electrolytes on the redox behaviour of
722 Cu(II) in aqueous medium, J. Bangladesh Chem. Soc. 24 (2011) 158–164.
723 https://doi.org/10.3329/jbcs.v24i2.9704.

724 [61] A. Bagger, R.M. Arán-Ais, J. Halldin Stenlid, E. Campos dos Santos, L. Arnarson, K. Degn
725 Jensen, M. Escudero-Escribano, B. Roldan Cuanya, J. Rossmeisl, Ab Initio Cyclic
726 Voltammetry on Cu(111), Cu(100) and Cu(110) in Acidic, Neutral and Alkaline Solutions,
727 ChemPhysChem. 20 (2019) 1–11. https://doi.org/10.1002/cphc.201900509.

728

729

730 Supplementary Information

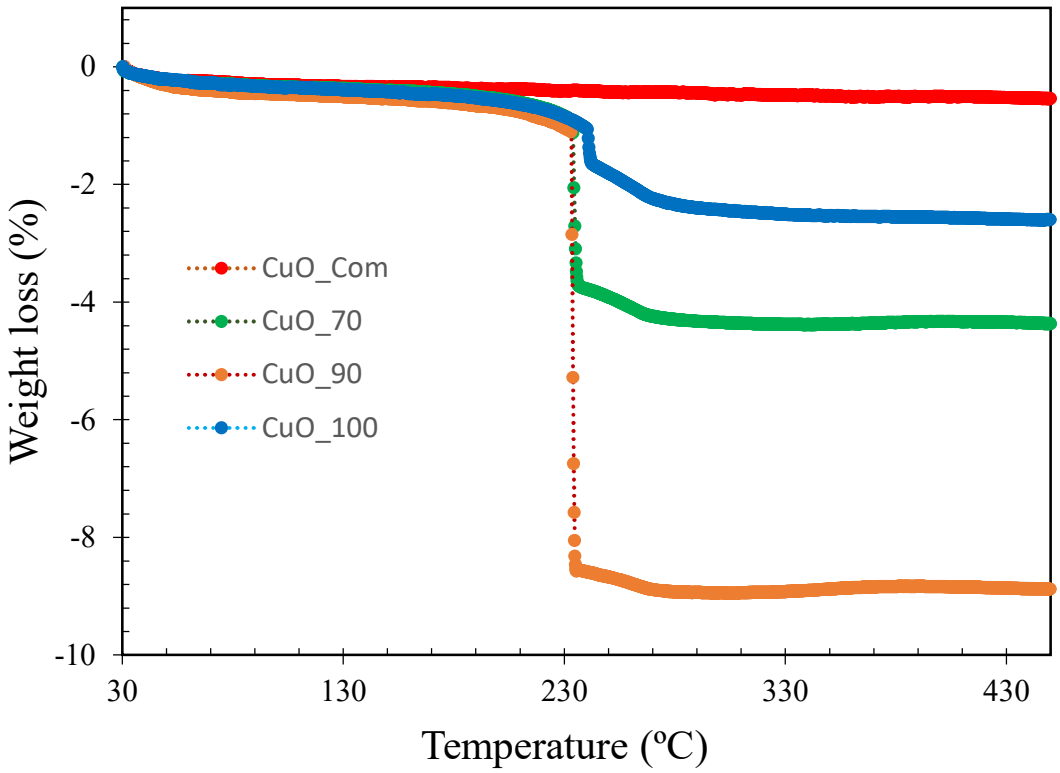

731

732 **Fig. S1**. Thermogravimetric analyses of commercial and synthesized CuO nanoparticles.

733

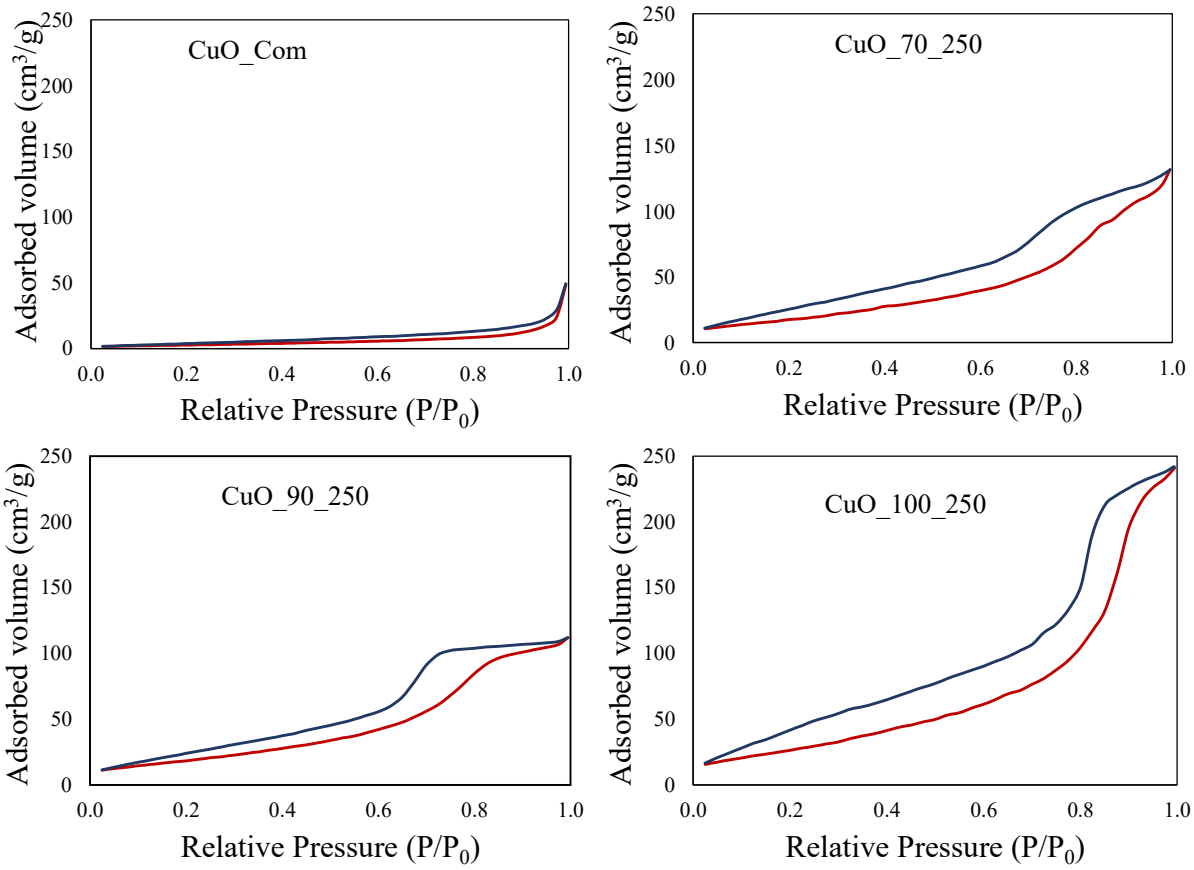

734

735 **Fig. S2**. Nitrogen adsorption-desorption isotherms corresponding to commercial and synthesized
736 CuO solids.

737

738

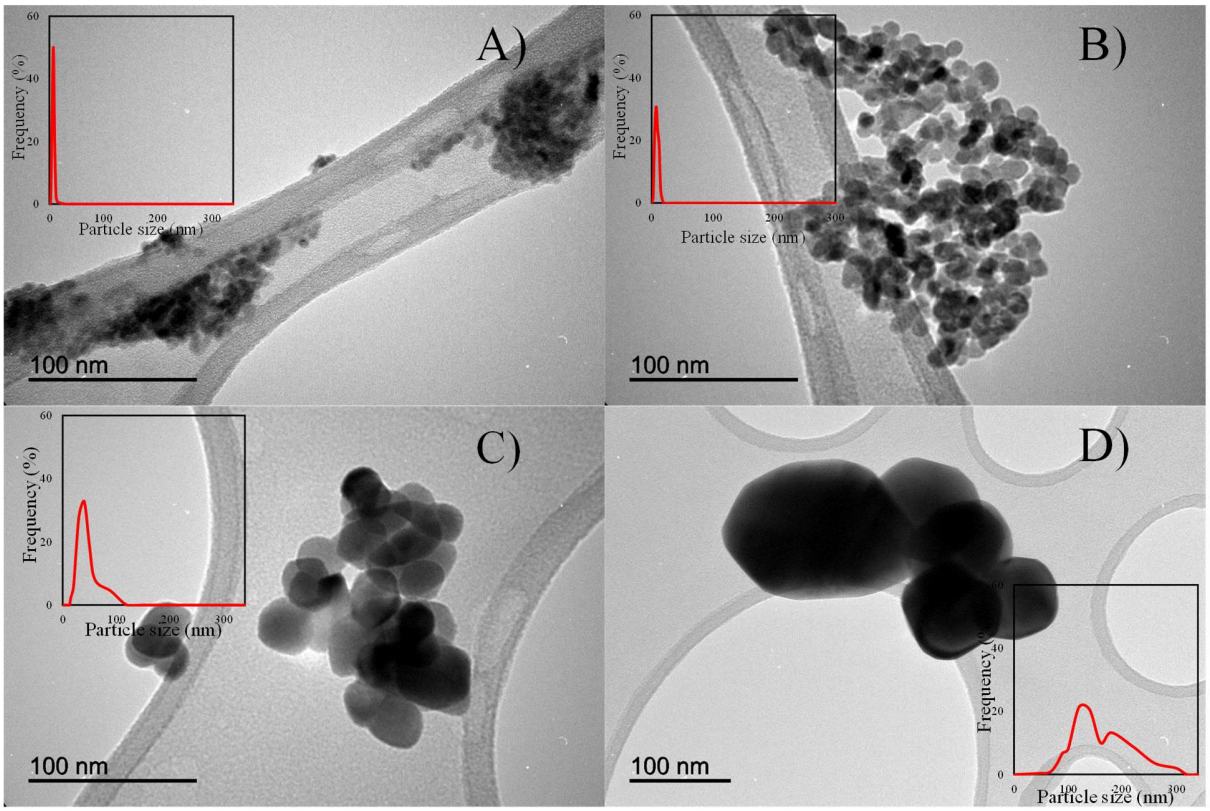

739

740 **Fig S3.** TEM images of A) CuO_100, B) CuO_100_250, C) CuO_100_450 and D) CuO_100_650.

741

742

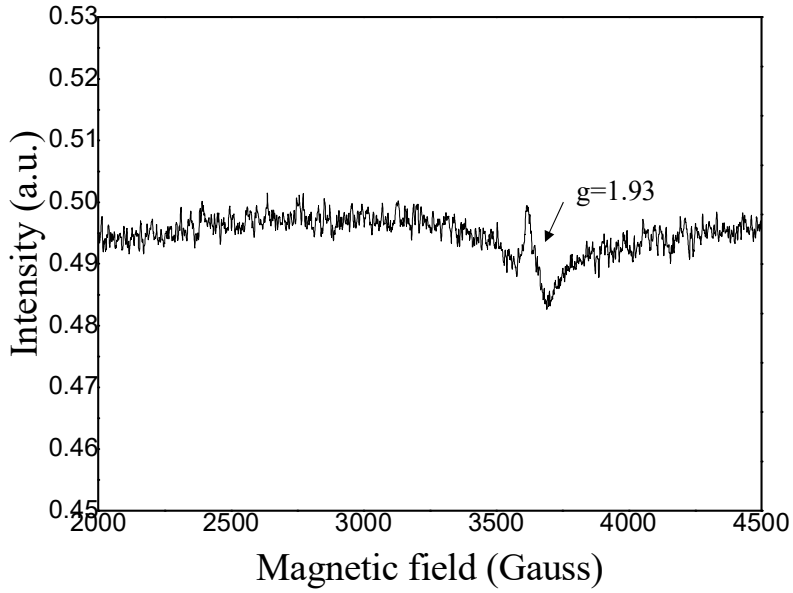

743

744 **Fig. S4**. EPR spectrum of a glycerol in water solution (10% v/v)

745

746

747

748

749

750

751

752

753

754

755

756

757